

Non-canonical amino acid incorporation into AAV5 capsid enhances lung transduction in mice

Hao Chang,^{1,5} Ailing Du,^{1,5} Jun Jiang,² Lingzhi Ren,¹ Nan Liu,¹ Xuntao Zhou,¹ Jialing Liang,¹ Guangping Gao,^{1,3} and Dan Wang^{1,4}

¹Horae Gene Therapy Center, University of Massachusetts Chan Medical School, Worcester, MA 01605, USA; ²GeneLeap Bio, Luye Life Sciences, Woburn, MA 01801, USA; ³Department of Microbiology and Physiological Systems, University of Massachusetts Chan Medical School, Worcester, MA 01605, USA; ⁴RNA Therapeutics Institute, University of Massachusetts Chan Medical School, Worcester, MA 01605, USA

Gene therapy using recombinant adeno-associated virus (rAAV) relies on safe, efficient, and precise *in vivo* gene delivery that is largely dependent on the AAV capsid. The proteinaceous capsid is highly amenable to engineering using a variety of approaches, and most resulting capsids carry substitutions or insertions comprised of natural amino acids. Here, we incorporated a non-canonical amino acid (ncAA), Nε-2-azidoethylloxycarbonyl-L-lysine (also known as NAEK), into the AAV5 capsid using genetic code expansion, and serendipitously found that several NAEK-AAV5 vectors transduced various cell lines more efficiently than the parental rAAV5. Furthermore, one NAEK-AAV5 vector showed lung-specific transduction enhancement following systemic or intranasal delivery in mice. Structural modeling suggests that the long side chain of NAEK may impact on the 3-fold protrusion on the capsid surface that plays a key role in tropism, thereby modulating vector transduction. Recent advances in genetic code expansion have generated synthetic proteins carrying an increasing number of ncAAs that possess diverse biological properties. Our study suggests that ncAA incorporation into the AAV capsid may confer novel vector properties, opening a new and complementary avenue to gene therapy vector discovery.

INTRODUCTION

Recombinant adeno-associated virus (rAAV) is currently the leading *in vivo* gene therapy delivery platform for preclinical and clinical applications.^{1,2} Attributing to its high transduction efficiency, broad tissue tropism, durable transgene expression, and clinically proven safety profile, rAAV gene therapy has shown encouraging outcomes in clinical trials targeting monogenic disorders,³ leading to regulatory approval of several AAV-based gene therapy drugs.^{4–6}

Notwithstanding the encouraging safety and efficacy outcomes for many genetic indications, rAAV-based gene therapy is facing several hurdles toward broader utilization, such as immunogenicity,^{7,8} durability of transgene expression,⁹ and difficulties in achieving tissue-specific delivery and requirement of high doses for certain applications. To overcome these limitations, AAV capsid development has been a major focus in gene therapy research. A variety of strategies are employed to generate novel AAV capsids with desired features,¹⁰

including isolation of natural serotypes from human and other species,¹¹ rational design enabled by understanding of structure-function relationships,^{12,13} directed evolution by DNA shuffling and random peptide insertion,^{14–17} *in silico* design,^{18,19} and their combinatorial approaches.^{20,21} These efforts continue to produce AAV vectors with increasing specificity and potency.

Most engineered AAV capsids comprise structural viral proteins (VPs) of canonical amino acids encoded by a modified AAV capsid gene (*Cap*). Others carry additional chemical decorations to redirect tropism or shield from neutralizing antibodies, among which genetic code expansion provides a versatile platform to engineer AAV capsid.^{13,22–25} In this approach, a non-canonical amino acid (ncAA) is incorporated into VPs via recoding a nonsense mutation in the *Cap* gene; the ncAA (e.g., Nε-2-azidoethylloxycarbonyl-L-lysine, also known as NAEK) harbors a chemical moiety that enables bio-orthogonal click reaction with a ligand, thereby allowing site-specific ligand conjugation on capsid surface.^{13,22,23,25} As a result, an additional purification step following click reaction is necessary to remove unconjugated ligand, increasing the complexity and cost associated with vector manufacturing. Furthermore, the stoichiometry of conjugation needs careful optimization and characterization because it may impact on AAV capsid stability, integrity, and function.

In this study, we used genetic code expansion to generate a series of AAV5 vectors bearing NAEK. We chose to engineer the AAV5 capsid because recent studies showed that it has a favorable immunological profile in clinical applications.²⁶ Surprisingly, we found that some NAEK-modified AAV5 (NAEK-AAV5) vectors exhibited enhanced cell transduction efficiency compared with the parental AAV5 vector

Received 14 June 2023; accepted 4 October 2023;
<https://doi.org/10.1016/j.omtm.2023.101129>.

⁵These authors contributed equally

Correspondence: Guangping Gao, Horae Gene Therapy Center, University of Massachusetts Chan Medical School, Worcester, MA 01605, USA.

E-mail: guangping.gao@umassmed.edu

Correspondence: Dan Wang, Horae Gene Therapy Center, University of Massachusetts Chan Medical School, Worcester, MA 01605, USA.

E-mail: dan.wang@umassmed.edu



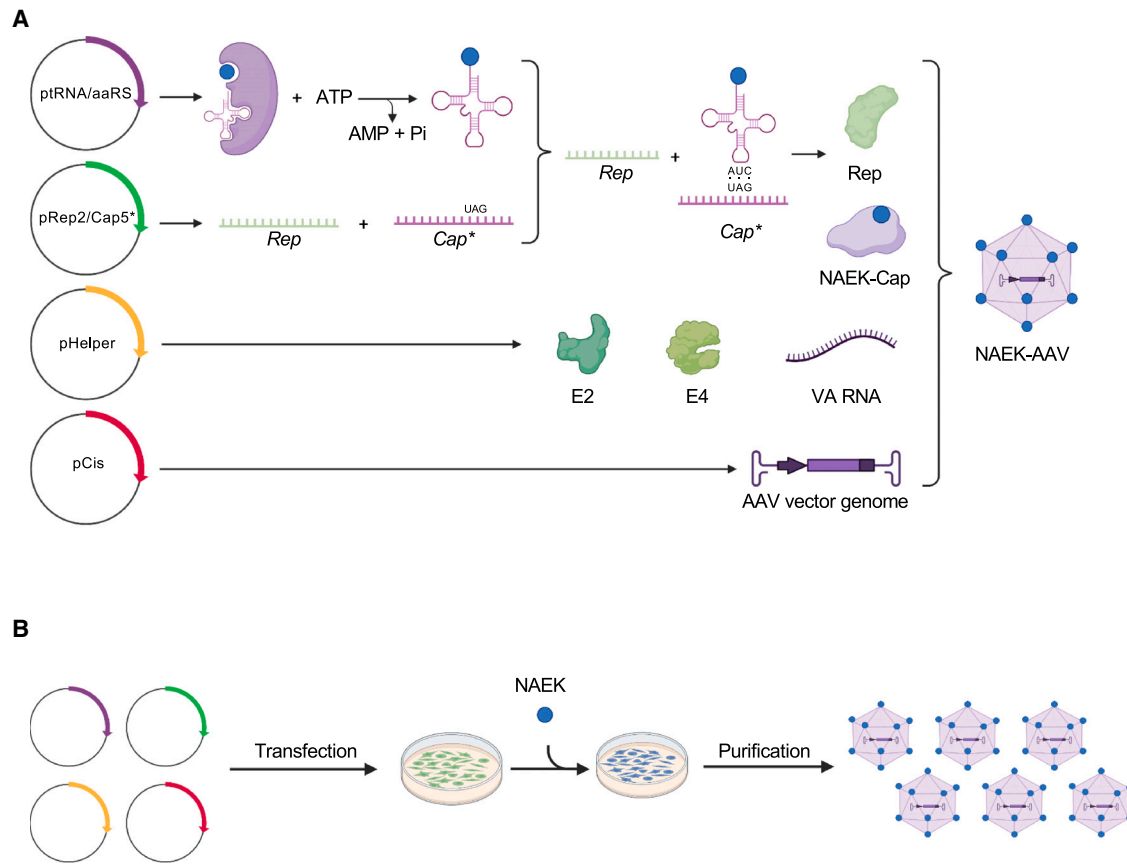


Figure 1. Schematic diagram showing NAEK incorporation into the AAV capsid during vector production

(A) NAEK (blue dot) is incorporated into the capsid via suppression of a premature termination codon in the *Cap* mRNA (*Cap**), also known as genetic code expansion. With adenoviral gene products from pHelper, the transgene cassette flanked by inverted terminal repeats in pCis is packaged into the modified rAAV capsid harboring NAEK at a specific site of the capsid surface. (B) Workflow of the NAEK-AAV vector packaging process. Four plasmids are co-transfected into HEK293 cells, and NAEK is added to the culture medium. NAEK-AAV vectors are then purified using the same procedure for regular rAAV.

without further conjugation to a ligand. In particular, NAEK substitution of VP residue 374D (i.e., 374NAEK) confers lung-specific transduction enhancement in mice. Structural modeling studies indicate that the long side chain of NAEK may alter a critical receptor binding region of the AAV5 capsid, thereby modulating tropism and transduction.

Recent advances in genetic code expansion technology allow a variety of ncAAs to be incorporated during protein synthesis.²⁷ These ncAAs possess diverse physical and chemical properties that are not present in natural amino acids, and can functionalize the synthetic protein products for a range of research and therapeutic applications.²⁸ Our study suggests that non-ncAA incorporation is a promising approach to AAV capsid engineering.

RESULTS

Generation of NAEK-AAV5 vectors and screen for packaging yield

We used genetic code expansion to incorporate NAEK into specific sites of AAV5 capsid during vector production (Figure 1A). Specif-

ically, a nonsense mutation was introduced into the AAV capsid gene (*Cap**), resulting in *Cap** mRNA bearing a UAG premature termination codon. The UAG was decoded by an orthogonal suppressor tRNA system that comprises the pyrrolysyl-tRNA synthetase/pyrrolysyl-tRNA pair and NAEK, thereby incorporating NAEK into VPs during translation. In the presence of adenoviral helper genes, the NAEK-AAV5 capsid encapsidates a recombinant AAV vector genome that expresses enhanced green fluorescent protein (EGFP) as a reporter. NAEK-AAV5 vectors were purified in the same way as for standard rAAV5 (Figure 1B).

Ten VP amino acid residues across variable regions (VRs) III to VIII were selected for NAEK engineering (Figure S1) because VRs were shown to impact on rAAV tropism.²⁹ NAEK was incorporated as either a substitution of a single residue or an insertion downstream (Figure 2A), generating a total of 20 NAEK-AAV5 vector designs. Next, we performed a small-scale vector production assay,³⁰ and found that NAEK modification generally compromised or abolished packaging yield, consistent with a previous report.²⁵ However, a few NAEK-AAV5 vectors exhibited packaging yield close to or more

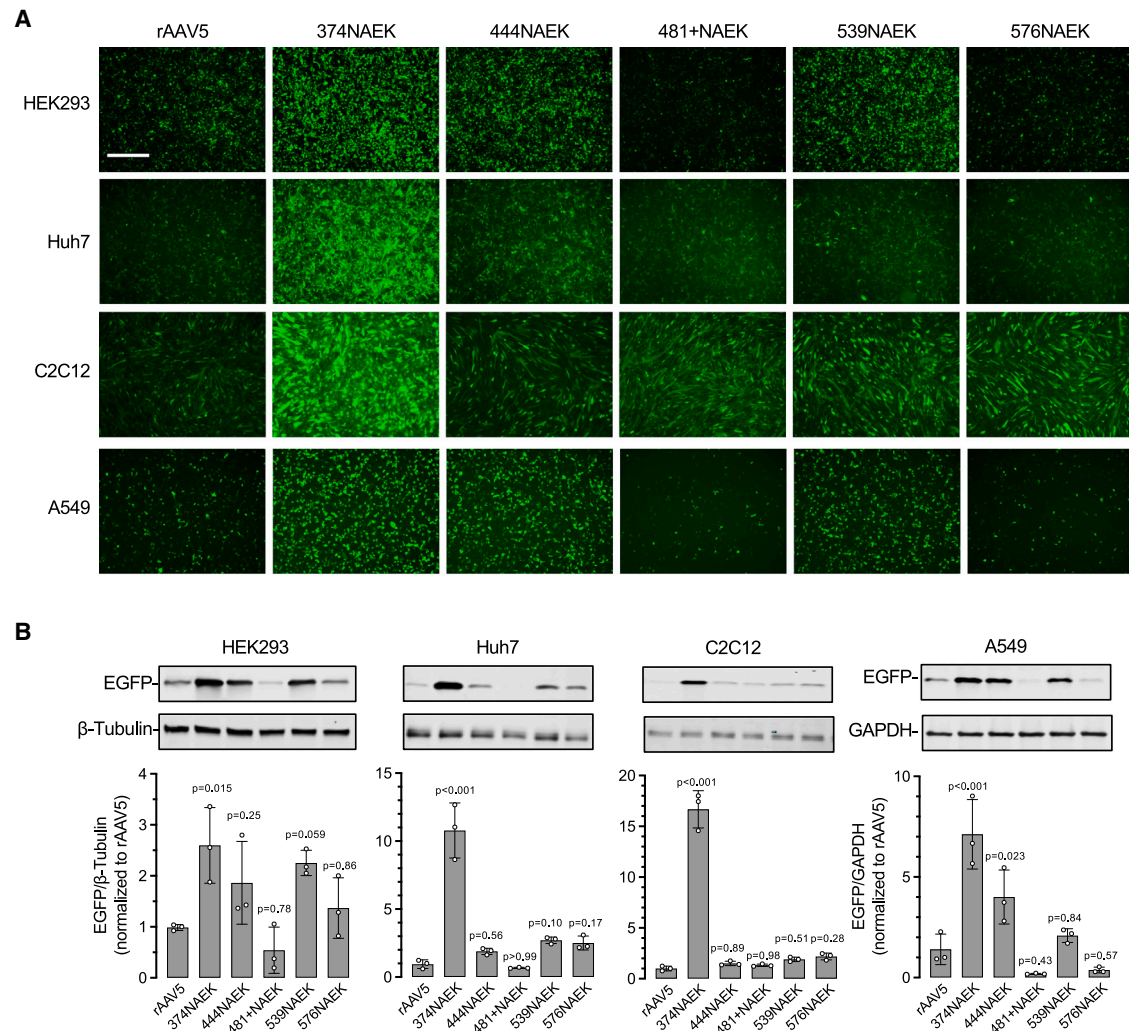


Figure 3. Transduction of various cell lines by selected NAEK-AAV5 vectors

(A) Fluorescence microscopy images of various cell lines transduced by unmodified rAAV5 or rAAV5 carrying the indicated NAEK modifications. All rAAVs package the same transgene cassette that expresses enhanced green fluorescent protein (EGFP). Cells were infected with each rAAV at a multiplicity of infection (MOI) of 50,000 with co-infection of adenovirus type 5 (AdV5) at a MOI of 100. Scale bar, 500 μ m. (B) Representative western blotting images of protein expression from cells as described in (A), and quantification of EGFP protein expression normalized to either β -tubulin or GAPDH. Data are normalized to the rAAV5 group. Data are mean \pm SD.

comparable with rAAV5 for targeting the liver, heart, and skeletal muscle, indicating tissue-specific transduction enhancement upon *in vivo* delivery. To further confirm the enhanced lung-targeting capacity of 374NAEK-AAV5, total lung protein was extracted and subjected to western blotting. Indeed, 374NAEK-AAV5-treated mice showed nearly 8-fold higher EGFP protein expression in the lung than those receiving rAAV5 (Figure 4D).

Encouraged by 374NAEK-AAV5's superb lung transduction following systemic delivery, we next performed intranasal instillation to study its lung tropism in mice (Figure 5A) because intranasal delivery of rAAV was shown to target the lung more efficiently than intravenous delivery.³¹ Following this localized treatment regimen

(Figure 5A), 374NAEK-AAV5 also outperformed the other vectors to target the lung, reaching 3- and 6-fold higher transgene EGFP expression than rAAV5 at mRNA and protein levels, respectively, although difference in transgene DNA abundance among all vectors did not reach statistical significance (Figure 5B). Taken together, these results demonstrate that NAEK incorporation at a specific site of the AAV5 capsid (i.e., residue 374) can enhance *in vivo* transduction in a tissue-specific manner.

Characterization of lung tropism of leading NAEK-AAV5 vectors

To further characterize the lung tropism, another cohort of mice receiving intranasal instillation of rAAV5 or 374NAEK-AAV5 were euthanized at a longer time point of 4 weeks post treatment (Figure 6A),

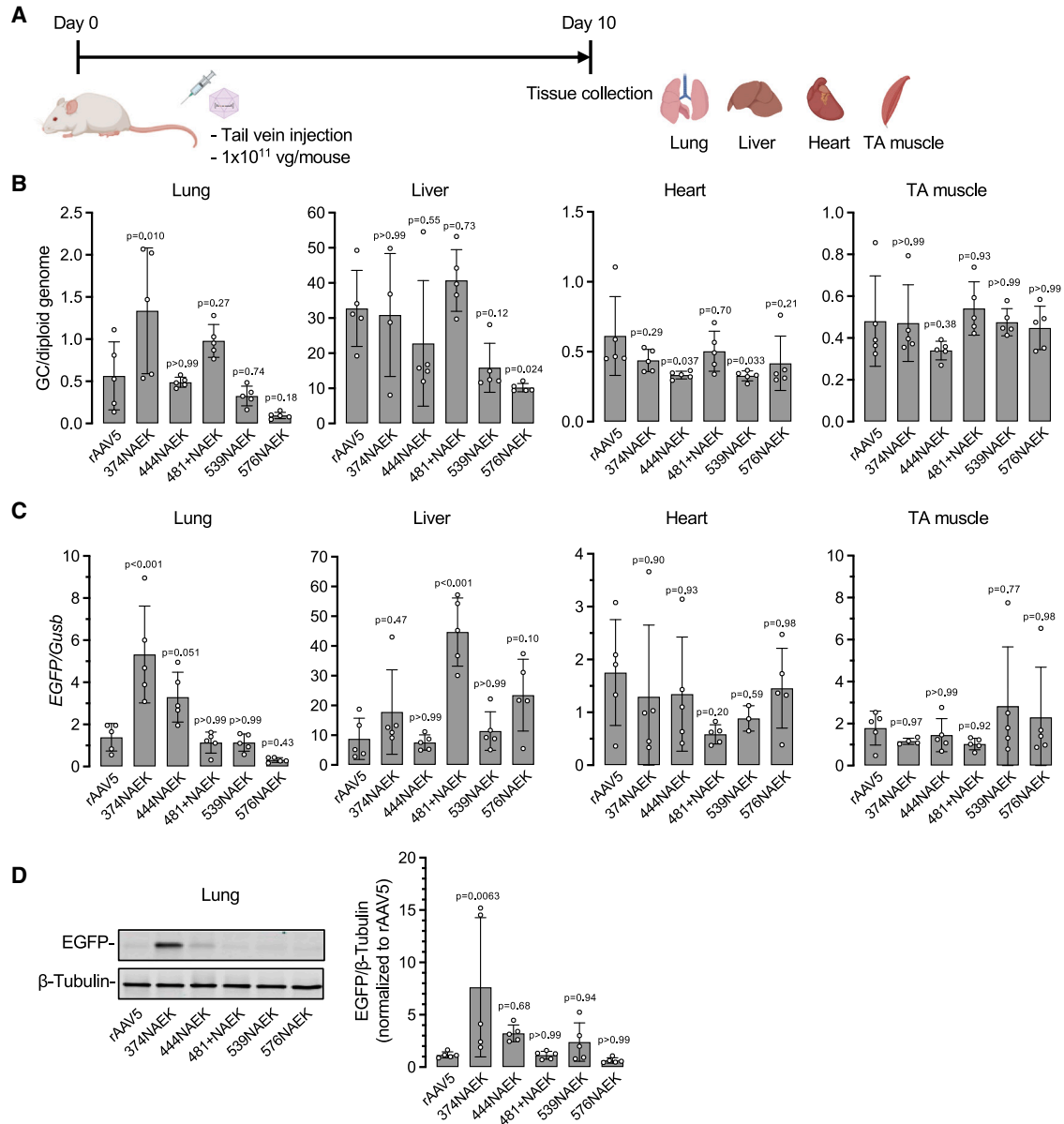


Figure 4. In vivo transduction by selected NAEK-AAV5 vectors in mice via systemic administration

(A) Schematic diagram of workflow. Six-week-old female mice were injected with rAAV at a dose of 1×10^{11} vector genomes (vg) per mouse via tail vein. Lung, liver, heart, and tibialis anterior (TA) muscle were collected 10 days post injection. (B) ddPCR quantification of rAAV transgene (i.e., *EGFP*) genome copy (GC) number in lung, liver, heart, and TA muscle of the mice described in (A). (C) ddPCR quantification of *EGFP* cDNA reverse-transcribed from its mRNA in lung, liver, heart, and TA muscle of the mice described in (A). (D) Representative western blotting images and quantification of transgene EGFP protein expression in lungs of the mice described in (A). Data are shown as mean \pm SD; each white dot represents an individual mouse. $n = 3$ –5 mice per group.

when rAAV transgene expression plateaued and stabilized.³² In addition, we also included 444NAEK-AAV5 in this experiment, because it repeatedly showed a trend of higher transgene expression than rAAV5 in prior experiments (Figures 3B, 4C, 4D, and 5B). Molecular analysis (Figure 6B) and immunostaining of lung sections (Figure 6C) corroborated the previous finding that 374NAEK-AAV5 led to the highest *EGFP* transgene expression in the lung.

Furthermore, we investigated the major lung cell types targeted by rAAV5 or the two NAEK-AAV5 vectors. Immunostaining results showed that most EGFP fluorescence was co-localized with pro-SPC, a specific marker of alveolar type 2 cells³³ (Figure 6D). 374NAEK-AAV5 not only led to 3-fold higher transgene expression than rAAV5, but also transduced more alveolar type 2 cells than rAAV5 (60% vs. 35%) (Figure 6D). In contrast, EGFP expression

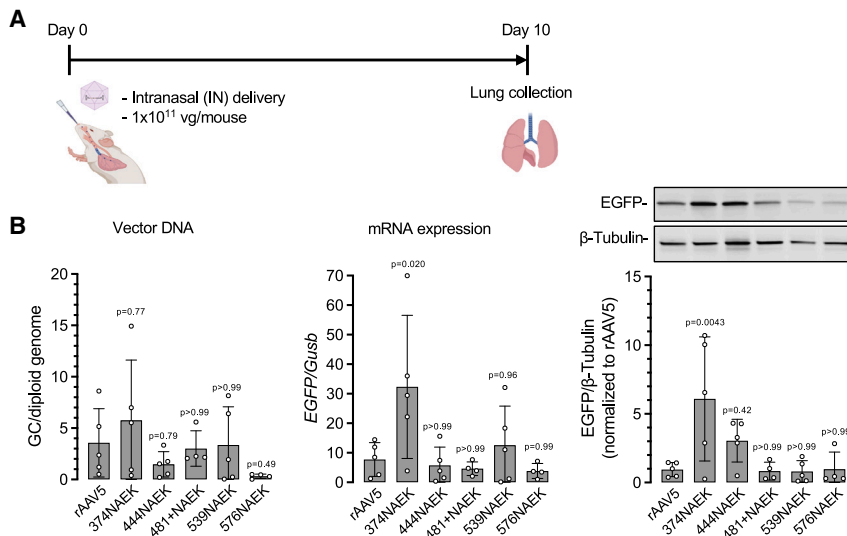


Figure 5. *In vivo* transduction by selected NAEK-AAV5 vectors in mice via intranasal administration

(A) Schematic diagram of workflow. Six-week-old female mice were injected with rAAV at a dose of 1×10^{11} vg per mouse via intranasal instillation. Lungs were collected 10 days post injection. (B) Quantification of rAAV vector DNA, transgene expression of mRNA, and EGFP protein expression in lung of the mice described in (A). Representative western blotting images of transgene EGFP protein expression are shown. Data are shown as mean \pm SD; each white dot represents an individual mouse. $n = 4-5$ mice per group.

from all vectors was rarely co-localized with the alveolar type 1 cell marker podoplanin (Figure S2). Importantly, neither 374NAEK-AAV5 nor 444NAEK-AAV5 triggered discernible inflammatory responses or histological changes to the lung (Figure 6E), suggesting that NAEK-AAV vectors were well tolerated despite the unnatural side chain of NAEK.

NAEK is a lysine (K) mimic (Figure 7A). To test whether the D374K substitution would confer the same lung tropism as D374NAEK, we performed intranasal instillation to another cohort of mice with various vectors (Figure 7B). However, 374K-AAV5 showed comparable lung transduction with rAAV5, both of which were inferior to 374NAEK-AAV5 (Figure 7C). Previous studies showed that rAAV6 and its two derivatives, rAAV6.2 and rAAV6.2FF, could transduce alveolar and airway epithelium in mice following intranasal or intratracheal delivery.³⁴⁻³⁶ Therefore, we also included these vectors for comparison and found that they were not as efficient as 374NAEK-AAV5 for lung transduction (Figure 7C). As expected, liver and heart contained much less vector DNA than the lung, presumably caused by vector leakage following intranasal delivery, and the transgene mRNA expression in the liver and heart was largely comparable among all tested vectors and much lower than that in the lung (Figures 7D and 7E).

Mechanistic studies on NAEK incorporation and vector properties

To explore the mechanisms underlying the enhanced lung transduction by 374NAEK-AAV5, we characterized its cellular trafficking in the human lung epithelial cell line A549 and compared it against rAAV5 and other NAEK-AAV5 vectors. In this set of *in vitro* experiments, 374NAEK-AAV5 exhibited the highest cell surface binding capacity and the most efficient internalization among all tested vectors (Figures 8A and 8B). After cell entry, 374NAEK-AAV5 delivered the greatest total number of vector DNA copies to nuclei, where transgene expression took place (Figure 8C). Notably, this cellular trafficking pattern was unique to 374NAEK-AAV5 but not the other

NAEK-modified vectors, indicating that the structural context of NAEK incorporation played a key role in determining vector property.

Residue 374 resides in VR-III, which is remote from the 3-fold protrusion, a capsid structural feature determining receptor binding and tropism.²⁹ However, we noticed that VR-III is spatially close to a β turn near the 3-fold axis (Figure 8D). When various amino acids (D, K, and NAEK) were fitted at residue 374 by structural modeling, only 374NAEK was in proximity with 498E in the neighboring β turn owing to its long side chain (Figure 8E), potentially forming hydrogen bonds between the two residues (Figure 8F). Thus, we postulate that the potential interaction between 374NAEK and 498E induces conformational changes near the 3-fold axis, thereby modulating the tropism of the 374NAEK-AAV5 vector.

DISCUSSION

In this study, we show that incorporation of a ncAA (i.e., NAEK) into the AAV5 capsid can modulate vector transduction. In particular, the 374NAEK-AAV5 vector exhibits lung-specific transduction enhancement in mice by either systemic injection or intranasal instillation, and significantly outperforms leading lung-tropic AAV capsids including AAV5, AAV6, and certain AAV6 variants. Our study suggests that ncAA incorporation is a viable approach to improving AAV vector tropism, expanding the arsenal of novel capsid discovery strategies.

A variety of ncAAs have been used to modify recombinant proteins as research tools. For example, Seidel et al. incorporated the photocrosslinking amino acid p-azido-Phe (Azi) into various sites of class B G-protein-coupled receptors (GPCRs). When a peptide antagonist binds to the Azi-GPCR and locates in proximity to the Azi residue, crosslinking occurs upon UV light activation, which reveals the detailed interaction between GPCR and peptide antagonists including the structural footprints and contact sites.³⁷ To our knowledge, ncAA incorporation into the proteinaceous AAV capsid for gene therapy vector development has been largely relying on NAEK as a chemical handle, followed by ligand conjugation via click reaction.^{13,22,24,25} Alternatively, the capsid surface-exposed amino acid side chains can be directly modified by chemical approaches.³⁸⁻⁴⁰ For example,

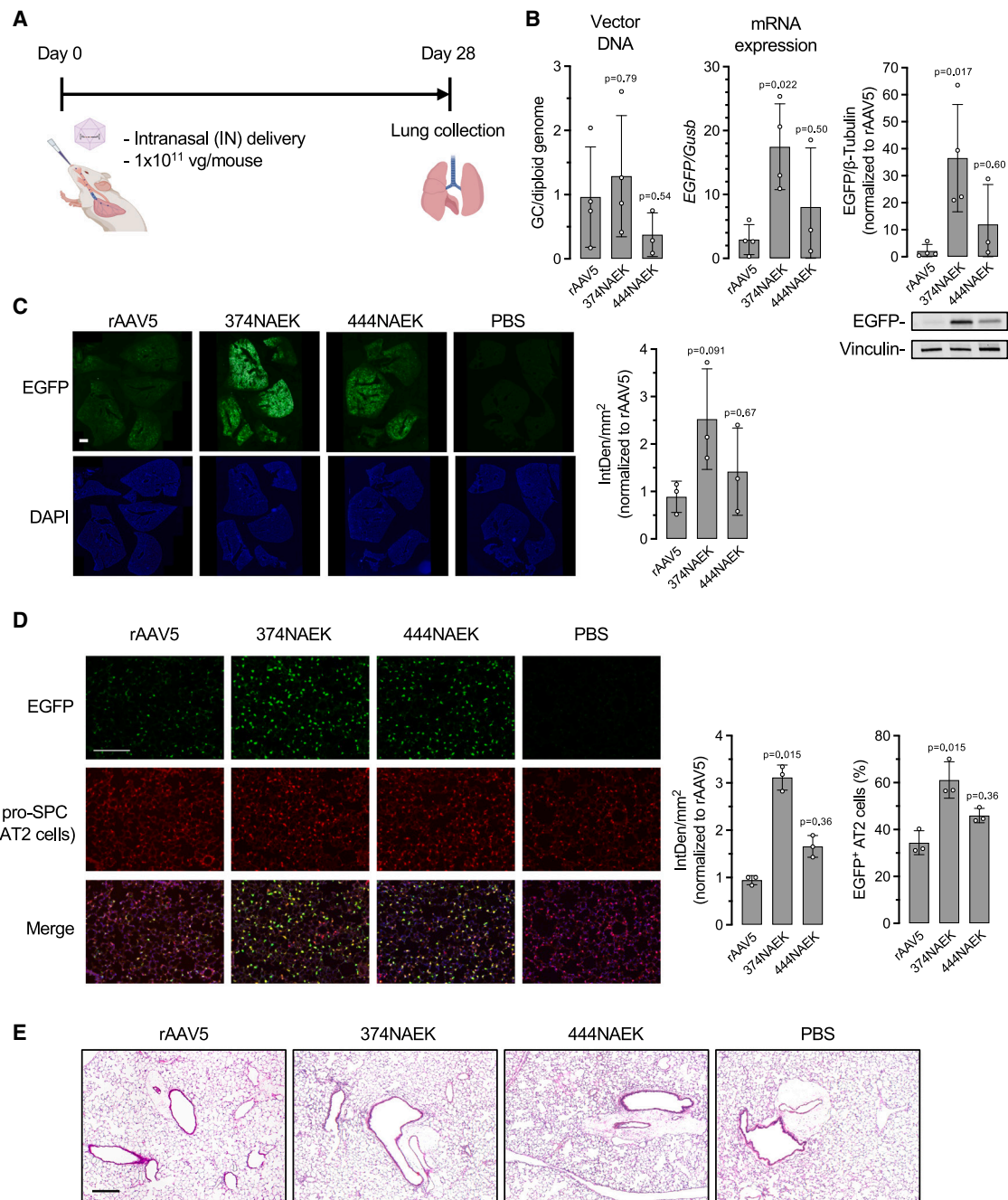


Figure 6. Characterization of lung transduction by two NAEK-AAV5 vectors via intranasal administration

(A) Schematic diagram of workflow. Six-week-old female mice were injected with rAAV at a dose of 1×10^{11} vg per mouse via intranasal instillation. Lungs were collected 28 days post injection. (B) Quantification of rAAV vector DNA, transgene expression of mRNA, and EGFP protein expression in lungs of mice described in (A). Representative western blotting images of transgene EGFP protein expression are shown. (C) Representative fluorescence microscopy images of lung sections and quantification of EGFP immunofluorescence intensity. Five lobes of one mouse are shown in each image. IntDen, integrated density of EGFP signal. Scale bar, 1 mm. (D) Representative fluorescence immunostaining images of lung sections and quantification. Alveolar type 2 (AT2) cells are labeled with antibody against pro-SPC (red). The fraction of EGFP⁺ AT2 cells is calculated as the percentage of EGFP⁺ pro-SPC⁺ double-positive cells among pro-SPC⁺ cells. Scale bar, 200 μ m. (E) Representative images of hematoxylin and eosin (H&E) staining of lung sections from mice administered with the indicated rAAV. Data are shown as mean \pm SD; each white dot represents an individual mouse. n = 3–4 mice per group. In (D) the Kruskal-Wallis test was used followed by Dunn's test against the rAAV5 group, because the data did not pass normal distribution test.

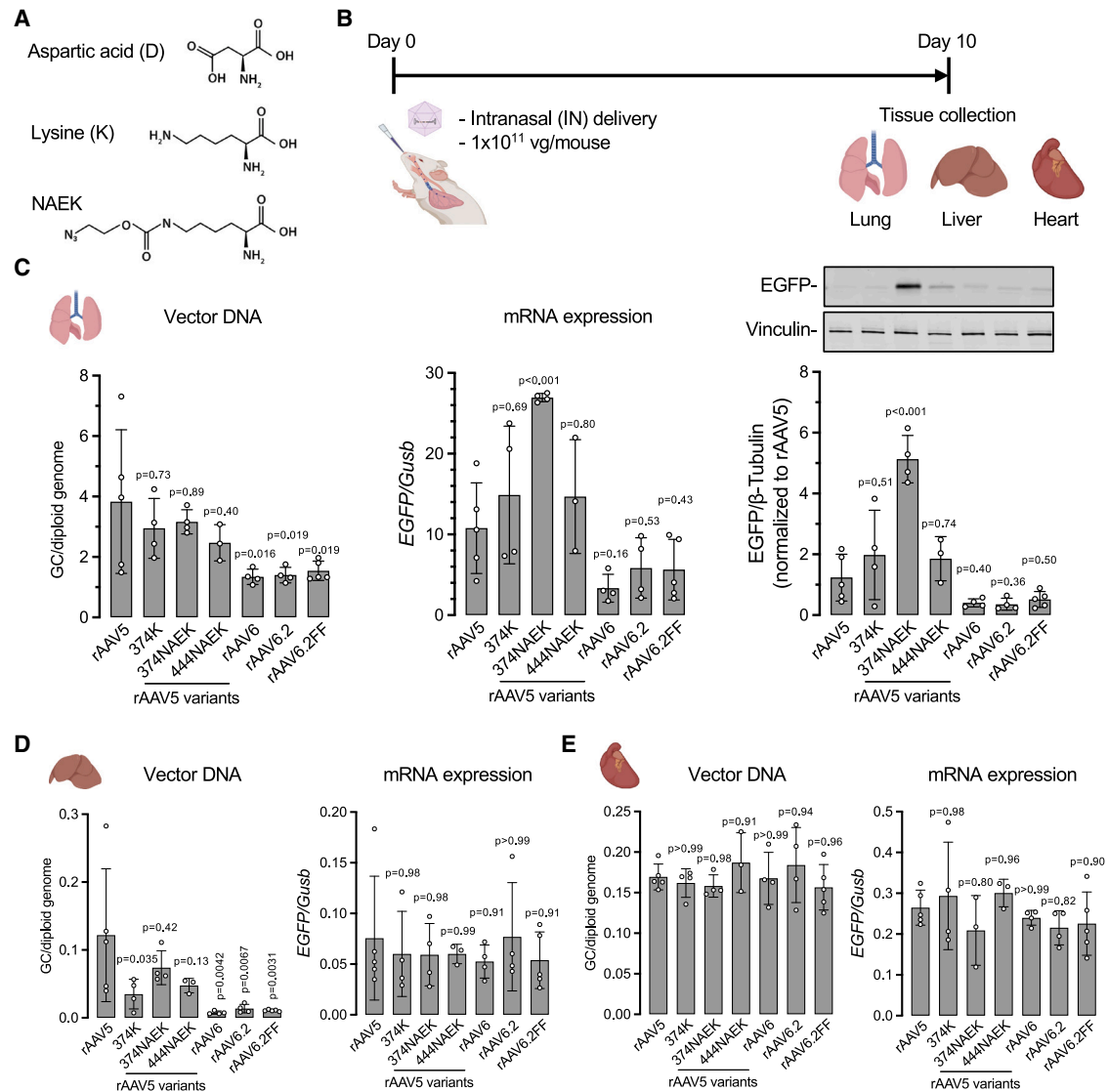


Figure 7. Comparison between NAEK-AAV5 vectors and other AAV vectors for *in vivo* transduction

(A) Chemical structures of canonical amino acids aspartic acid (D) and lysine (K) and the non-canonical amino acid NAEK. (D) The wild-type amino acid at residue 374 of AAV5 VP1. (B) Schematic diagram of workflow. Six-week-old female mice were injected with rAAV at a dose of 1×10^{11} vg per mouse via intranasal instillation. Lung, liver, and heart were collected 10 days post injection. (C) Quantification of rAAV vector DNA, transgene expression of mRNA, and EGFP protein expression in lungs of mice described in (B). Representative western blotting images of transgene EGFP protein expression are shown. (D) Quantification of rAAV vector DNA and transgene expression of mRNA in livers of mice described in (B). (E) Quantification of rAAV vector DNA and transgene expression of mRNA in hearts of mice described in (B). Data are shown as mean \pm SD; each white dot represents an individual mouse. $n = 3$ –5 mice per group.

Horowitz et al. modified AAV2 arginine residues to the neutral adduct hydroimidazolone by glycation, which redirected the vector tropism from liver to skeletal and cardiac muscle in mice by systemic administration.³⁸

The simplicity of one-step ncAA incorporation without a downstream chemical reaction sets our study apart from the aforementioned methods for capsid engineering. Therefore, manufacturing ncAA-AAV vectors is very similar to standard rAAV production, whereas

a two-step capsid modification method requires an additional purification procedure, which increases the complexity and cost of vector manufacture and may decrease yield. Importantly, ncAA incorporation occurs via genetic code expansion at a pre-defined premature termination codon, and therefore is precise and consistently generates a homogeneous batch of vectors. In contrast, decorating purified rAAV via either click reaction or other chemical approaches usually results in incomplete modification and/or unspecific modification at multiple residues, consequently producing inconsistent vector batches.

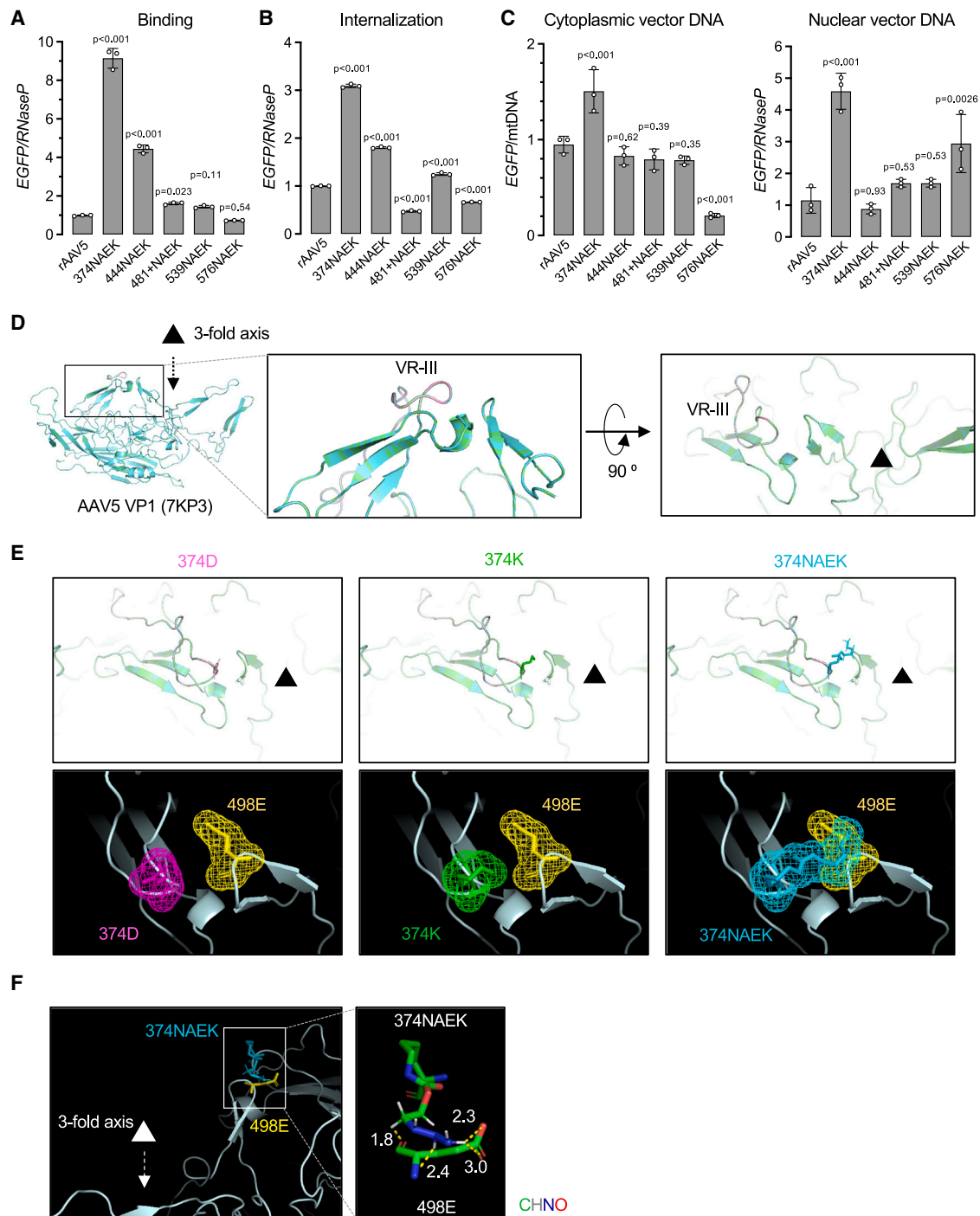


Figure 8. Mechanistic studies of the impact of NAEK incorporation on vector properties

(A) Comparison between rAAV5 and five NAEK-AAV5 vectors for their binding capacity to A549 cells (a human lung epithelial cell line). (B) Comparison between rAAV5 and five NAEK-AAV5 vectors for their internalization efficiency in A549 cells. (C) Comparison between rAAV5 and five NAEK-AAV5 vectors for their cytoplasmic and nuclear distribution in A549 cells. (D) Ribbon diagram of AAV5 VP1 monomer (PDB: 7KP3). The position of the 3-fold axis is indicated by a black triangle. Enlarged views show the VR-III-containing residue 374D and the neighboring β turn. (E) Ribbon diagrams (top panels) showing three amino acids at residue 374D (purple), 374K (green), and 374NAEK (cyan). In the bottom panels, electron density maps of 374D (purple), 374K (green), 374NAEK (cyan), and their neighboring amino acid 498E (yellow) are shown as a colored mesh. (F) Interatomic distances (in angstroms and indicated by dashed lines) between 374NAEK (cyan) and 498E (yellow) are labeled.

We identified 374NAEK-AAV5 as a potent vector to target lung alveolar type 2 cells in mice. AAV-based gene therapy is regarded as a promising therapeutic modality to treat a range of lung diseases, such as cystic fibrosis, and several lung-targeting AAV capsids have been reported.^{35,41} For example, Limberis et al. compared AAV serotypes 1–9 for their lung transduction efficiency in mice, and found that AAV5 and AAV6 were among the most efficient. Furthermore, they demonstrated that AAV6.2, an AAV6 F129L mutant, outperformed the other serotypes tested to transduce mouse lung epithelium.³⁵ Transduction efficiency of rAAV6.2 was approximately 2-fold higher than the parental rAAV6 in both airways and alveoli.³⁴ Introducing Y455F and Y731F substitutions to AAV6.2 yielded AAV6.2FF, which was shown to further increase transgene expression in muscle and lung, presumably due to reduced proteasomal degradation of the capsid.³⁶ Notably, 374NAEK-AAV5 vector showed higher lung transduction efficiency than AAV5, AAV6, AAV6.2, and AAV6.2FF vectors 10 days after intranasal delivery, suggesting that 374NAEK-AAV5 is a promising gene therapy vector targeting the lung, especially for gene delivery to alveolar type 2 cells that are involved in diseases such as surfactant B deficiency.⁴² Future translational studies may evaluate cell-type-specific transgene expression over a longer time course and tropism in non-human primates. It is also important to assess potential immune responses against nAA and possible new epitopes harboring nAA. We note that other AAV capsids, such as AAV4⁴³ and an engineered AAV9-derived capsid,⁴⁴ exhibit promising lung transduction in mice following intravenous delivery and hold promise in clinical translation.

Our comparative studies on several NAEK-AAV5 vectors indicate that both NAEK incorporation and its insertion site (and hence structural context) play a role in modulating transduction efficiency and intracellular trafficking. Consistent with this notion, structural modeling reveals the potential interaction between 374NAEK and 498E that resides near the 3-fold protrusion, a critical structural determinant of tropism. This interaction is enabled by the long side chain of NAEK that does not exist in canonical amino acids, including the wild-type aspartic acid (D) or lysine (K). Detailed interatomic interactions and conformational changes caused by 374NAEK substitution will require structural analysis such as cryo-EM and three-dimensional reconstruction. Moreover, how these interaction changes impart enhanced cellular transduction also warrants further investigation. Our *in vitro* study using A549 cells indicates that 374NAEK substitution confers stronger vector binding to the cell surface, eventually leading to higher nuclear vector DNA. However, we note that 374NAEK-AAV5 may exhibit enhanced lung transduction via a different mechanism once delivered *in vivo*. Nevertheless, these results support the conclusion that incorporation of nAA with a synthetic side chain may confer novel AAV capsid properties that are not readily achievable by the limited canonical amino acids.

To identify nAA-AAV vectors of desired properties more efficiently and rapidly, it is plausible to synergize with a library screening approach.^{45,46} Alternatively, rational design to incorporate specific nAAs with desired biological characteristics may also functionalize

the resulting vectors. As advances in genetic code expansion make an increasing number of nAAs amenable to synthetic protein production, the diverse nAA-AAVs may provide an untapped yet rich repertoire for gene therapy vector discovery.

MATERIALS AND METHODS

Cell culture

HEK293 cells (cat. no. CRL-1573), C2C12 cells (cat. no. CRL-1772), and A549 cells (cat. no. CRM-CCL-185) were purchased from ATCC. Huh7 cells were obtained from Wen Xue as a gift. All cells were maintained in Gibco Dulbecco's modified Eagle's medium (DMEM) (Thermo Fisher Scientific, cat. no. 11965-084) supplemented with 10% fetal bovine serum (FBS) and 1% penicillin/streptomycin (culture medium hereafter) under 37°C and 5% CO₂.

Small-scale AAV vector packaging assay

To generate pRep2/Cap5* plasmids, TAG nonsense mutations were introduced in the *Cap* gene by Gibson Assembly (New England BioLabs, cat. no. E2611) or site-directed mutagenesis (TaKaRa, cat. no. R045A) according to the manufacturer's instructions. Four plasmids (pAAVsc.PI-CB6-EGFP, pRep2/Cap5*, pHelper, and ptRNA/aaRS [Addgene, cat. no. 50832]) were co-transfected into HEK293 cells at a mass ratio of 1:1:1:2 using the calcium precipitation method (Promega, cat. no. E1200). After 12 h, culture medium was replaced with fresh medium containing 1 mM NAEK (Aquila Pharmatech, cat. no. SCI0043). At 72 h post transfection, cells were detached, suspended in the culture medium, and subjected to three successive freeze-thaw cycles. The crude lysates were centrifuged at 15,000 g/min for 15 min at 4°C to remove cell debris; supernatant was stored at –20°C. DNase-resistant rAAV titer in cleared crude lysate was determined by real-time quantitative PCR (qPCR) as described previously.³⁰

Large-scale AAV vector production

Similar to the small-scale AAV vector packaging process, the aforementioned four plasmids were co-transfected into HEK293 cells. After 12 h, culture medium was replaced with fresh DMEM containing 1 mM NAEK (Aquila Pharmatech, cat. no. SCI0043). At 72 h post transfection, AAV vectors were purified from crude lysates by CsCl gradient centrifugation followed by dialysis.⁴⁷ All AAV vectors packaged the same self-complementary vector genome expressing EGFP. Purified AAV vectors were quantified by droplet digital PCR (ddPCR) for vector genome titer and silver-stained SDS-PAGE analysis for purity assessment.

rAAV conjugation with DBCO-IRDye800 via click reaction

rAAV (2.5 × 10¹¹ vg) and DBCO-IRDye800 (LI-COR Biosciences, cat. no. 929–50000) was mixed at a molar ratio of 1:1,000 in 200 μL of Dulbecco's phosphate-buffered saline (DPBS) (pH 7.0) (Corning, cat. no. 21-031-CV) in a 1.5 mL microcentrifuge tube, and incubated at room temperature in darkness for 2 h. After click reaction, the mixture was purified using Amicon Ultra 100K filter (MilliporeSigma, cat. no. UFC510096) and reconstituted in 50 μL of DPBS.

rAAV transduction assay *in vitro*

Cells were seeded at a density of 2×10^5 to 4×10^5 cells/well in a 12-well plate. Next day, cells were co-infected with rAAV at a multiplicity of infection (MOI) of 50,000 and human adenovirus 5 (AdV5) at a MOI of 100. At 48 h (HEK293, Huh7, A549 cells) or 168 h (C2C12 cells) post infection, cells were subjected to fluorescence imaging to qualitatively detect EGFP expression. Another batch of cells were infected in the same way, and cell lysates were collected at 48 h post infection and subjected to western blotting to quantitatively measure transduction.

Animal use and treatment

Six-week-old female C57BL/6J mice were purchased from The Jackson Laboratory (Stock no. 000664). Mice were administered with AAV vectors at a dose of 1×10^{11} vg/mouse by either tail vein injection or modified intranasal instillation.³¹ After 10 or 28 days post treatment, mice were sacrificed for tissue collection. All animal experiments were reviewed and approved by the Institutional Animal Care and Use Committee of University of Massachusetts Chan Medical School.

rAAV vector DNA and transcript quantification

Flash-frozen tissues, including lung, liver, heart, and TA muscle, were subjected to total DNA and RNA extraction using AllPrep DNA/RNA Mini Kit (QIAGEN, cat. no. 80204). RNA was reverse-transcribed into cDNA using a cDNA Reverse Transcription Kit (Thermo Fisher Scientific, cat. no. 4374966). Vector DNA and cDNA were quantified using duplexing TaqMan ddPCR assays targeting *EGFP* (Thermo Fisher Scientific, Assay ID Mr00660654_cn) and *Tfrc* genomic sequences (Thermo Fisher Scientific, cat. no. 4458367), or *EGFP* and *Gusb* cDNA (Thermo Fisher Scientific, cat. no. 4448490), respectively. ddPCR was carried out using QX200 (Bio-Rad), and results were analyzed using QuantaSoft (Bio-Rad).

Western blotting

For rAAV5 conjugated with IRDye800, 1×10^{10} vg of rAAV purified using an Amicon filter was loaded in each lane for SDS-polyacrylamide gel electrophoresis (SDS-PAGE), followed by standard membrane transfer procedure. Membrane was then incubated with mouse anti-VP1/2/3 (B1) primary antibody (PROGEN, cat. no. 61058) at 4°C overnight and subsequently incubated with goat anti-mouse IgG polyclonal antibody-IRD-680RD secondary antibody (LI-COR, cat. no. 926-68070) at room temperature for 1 h. Membrane was imaged using a LI-COR Odyssey Imaging System and images were analyzed with Image Studio Lite Quantification Software (LI-COR).

To detect proteins in cells and tissues, total protein was extracted using Novex NP40 Cell Lysis Buffer (Thermo Fisher Scientific, cat. no. FNN0021) and T-PER Tissue Protein Extraction Reagent (Thermo Fisher Scientific, cat. no. 78510), respectively. Primary antibodies include rabbit anti-EGFP antibody (1:3,000, Thermo Fisher Scientific, cat. no. A-11122), rabbit anti-GAPDH antibody (1:3,000, Abcam, cat. no. ab9485), anti-vinculin antibody (1:5,000, Abcam, cat. no. ab219649), and mouse anti- β -tubulin antibody (1:5,000, Abcam,

cat. no. ab7291). Secondary antibodies include goat anti-mouse IgG polyclonal antibody-IRD-680RD and donkey anti-rabbit IgG polyclonal antibody-IRD-800RD (1:5,000, LI-COR, cat. no. 926-68070 and 926-32213, respectively).

Slot blotting

rAAV (1×10^{10} vg) was diluted in 150 μ L of DPBS and then loaded on a nitrocellulose membrane in a Blotting Manifold (Hoefer, PR648). After the rAAV suspension filtered through by gravity (\sim 30 min), blocking buffer (LI-COR, cat. no. 927-70003) was added onto the membrane and allowed to filter through by gravity (\sim 1 h). After blocking, the membrane was washed with DPBS three times using a vacuum. Washed membrane was incubated with mouse anti-AAV5 intact particle antibody (PROGEN, cat. no. 610148) at 4°C overnight. Subsequently, the membrane was incubated with goat anti-mouse IgG IRD-680RD secondary antibody at room temperature for 1 h, and imaged using a LI-COR Odyssey Imaging System.

SYPRO Ruby protein stain

Purified rAAVs and molecular weight markers (Bio-Rad, cat. no. 1610363) were subjected to SDS-PAGE as mentioned above. The gel was fixed in 50% methanol and 7% acetic acid for 60 min (two 30-min rounds), and incubated in SYPRO Ruby gel stain (Thermo Fisher Scientific, cat. no. S12000) overnight. Next day, gel was washed in 10% methanol and 7% acetic acid, rinsed in MilliQ water, and imaged using a GelDoc Go Gel Imaging System (Bio-Rad).

rAAV binding, internalization, and subcellular distribution analysis

rAAV binding and internalization assay was performed as previously reported⁴⁸ with minor modifications. In brief, A549 cells were seeded 18 h prior to assay. Cells were pre-chilled at 4°C for 30 min to stop endocytosis, infected with rAAV at a MOI of 67,000, and incubated at 4°C for 1 h. After incubation, cells were washed gently with cold DPBS three times to remove unbound rAAV. For binding assay, washed cells were harvested and subjected to total DNA isolation using QIAGEN AllPrep DNA/RNA Mini Kit. For internalization assay, after unbound vectors were removed, cells were incubated in warm culture medium at 37°C and 5% CO₂ for 1 h to allow rAAV endocytosis to occur. After incubation, cells were detached in 0.05% trypsin (Cytiva, cat. no. SV3003101) for 5 min followed by quenching with culture medium. Cell suspension was centrifuged and cell pellets were washed with DPBS three times followed by total DNA isolation using the QIAGEN AllPrep DNA/RNA Mini Kit.

Subcellular distribution of rAAV was analyzed as reported previously⁴⁹ with minor modifications. A549 cells were infected with rAAV at a MOI of 50,000 and harvested after 24 h. The cytoplasmic and nuclear fractions were isolated using an NE-PER Kit (Thermo Fisher Scientific, cat. no. 78833). Both fractions were subjected to duplexing TaqMan qPCR to quantify rAAV vector DNA distribution. Vector DNA was detected using a TaqMan reagent targeting the *EGFP* gene (Thermo Fisher Scientific, Assay ID Mr00660654_cn).

For nuclear fraction, a TaqMan reagent targeting the human *RNase P* gene (Thermo Fisher Scientific, TaqMan copy number assay ID 4331182) was chosen as a normalization reference of A549 genomic DNA. For cytoplasmic fraction, a TaqMan reagent targeting mitochondrial DNA (forward primer: CACCCAAGAACAGGGTTTGT; reverse primer: TGGCCATGGGTATGTTGTTA; probe: /5HEX/TTACCGGGC/ZEN/TCTGCCATCT/3IABkFQ/; synthesized by Integrated DNA Technologies) was used as normalization reference. The qPCR assays were performed using TaqMan Gene Expression Master Mix (Thermo Fisher Scientific, cat. no. 4369016) on a StepOne Real-Time PCR System (Thermo Fisher Scientific).

Immunofluorescence staining of lung sections

Mice were intratracheally perfused with fresh 4% paraformaldehyde (PFA). Lungs were dissected, fixed in 4% PFA for 24 h, and dehydrated in 15% sucrose in 1× PBS for 24 h. Dehydrated lung was embedded in a disposable mold containing OCT and flash frozen at -80°C for at least 24 h. Embedded lung was cut into 15 μm sections using a cryostat microtome and stored at -80°C . Sections on glass slides were permeabilized with 0.1% Triton X-100 in 1× PBS for 10 min and blocked with 5% donkey serum for 30 min, followed by primary antibody incubation at 4°C overnight and secondary antibody incubation at room temperature for 1 h. Primary antibodies used were anti-EGFP antibody (1:1,000, Aves Labs, cat. no. GFP1010), anti-podoplanin (1:500, Abcam, cat. no. ab11936), and rabbit anti-pro-SPC (1:1,000, MilliporeSigma, cat. no. AB3786). Secondary antibodies include goat anti-chicken IgY H&L Alexa Fluor 488 (1:1,000, Abcam, cat. no. ab150169) and goat anti-rabbit IgG (H + L) Alexa Fluor Plus 594 (1:1,000, Thermo Fisher Scientific, cat. no. 32740). Immunostained sections were mounted with ProLong Diamond Antifade Mountant (Thermo Fisher Scientific, cat. no. P36970) and subjected to imaging using a THUNDER Imaging System (Leica Microsystems, Germany). Fluorescence intensity was quantified and analyzed using ImageJ (National Institutes of Health).

Structural modeling of AAV capsid

The structure of intact 60-mer AAV5 capsid (PDB: 7KP3) was retrieved from RCSB PDB and VP monomer was displayed using PyMOL 2.4.1. The amino acid residues selected for NAEK substitution or insertion were pseudo-colored and mapped onto the VP monomer structure. The NAEK chemical structure was created using the Builder module of PyMOL. The Mutagenesis module of PyMOL was used to replace the wild-type 374 aspartic acid (D) to either lysine (K) or NAEK. Interatomic distance was measured using the measurement module of PyMOL.

Statistical analysis

Data are presented as mean \pm standard deviation (SD). Comparison among multiple groups was analyzed by one-way analysis of variance (ANOVA) followed by Dunnett's multiple comparison test against rAAV5 group, corrected for multiple comparison. GraphPad Prism 9 was used for statistical analysis and data plotting.

DATA AND CODE AVAILABILITY

All study data are included in the article and/or supplemental information.

SUPPLEMENTAL INFORMATION

Supplemental information can be found online at <https://doi.org/10.1016/j.omtm.2023.101129>.

ACKNOWLEDGMENTS

We wish to thank Qin Su for providing training on intratracheal perfusion, Mengtian Cui for generously sharing the TaqMan reagents detecting mitochondrial DNA, the Morphology Core Facility at UMass Chan for tissue sectioning and immunostaining, and the Viral Vector Core at UMass Chan for producing the AAV vectors used in this study. The Wang Lab is supported by a grant from the National Institutes of Health (NIH) (P01HL158506). The Gao Lab is supported by grants from the NIH (R01NS076991-01, P01AI100263-01, P01HL131471-02, 35 R01AI121135, UG3HL147367-01, R01HL097088, and U19AI149646-01) and the Cystic Fibrosis Foundation. Some illustrations were created with biorender.com.

AUTHOR CONTRIBUTIONS

H.C. and D.W. designed the research. H.C. carried out the majority of the experiments. H.C., A.D., X.Z., and J.L. performed mouse injection and other mouse work. J.J. provided NAEK and advice on its use. L.R., H.C., and N.L. did molecular cloning. L.R. and N.L. produced rAAV. H.C., D.W., and G.G. analyzed data and wrote the manuscript.

DECLARATION OF INTERESTS

This work was funded in part through a sponsored research agreement with Luye Pharma. J.J. was a paid employee of Luye Pharma. None of the other authors received personal compensation from Luye Pharma or hold financial interest in the company. H.C., A.D., G.G., and D.W. are inventors of a patent application filed by the University of Massachusetts Chan Medical School concerning the work described in this study. G.G. is a scientific co-founder of Voyager Therapeutics, Adrenas Therapeutics, and Aspa Therapeutics, and holds equity in the companies.

REFERENCES

- Hastie, E., and Samulski, R.J. (2015). Adeno-associated virus at 50: a golden anniversary of discovery, research, and gene therapy success—a personal perspective. *Hum. Gene Ther.* 26, 257–265.
- Wang, D., Tai, P.W.L., and Gao, G. (2019). Adeno-associated virus vector as a platform for gene therapy delivery. *Nat. Rev. Drug Discov.* 18, 358–378.
- Mendell, J.R., Al-Zaidy, S.A., Rodino-Klapac, L.R., Goodspeed, K., Gray, S.J., Kay, C.N., Boye, S.L., Boye, S.E., George, L.A., Salabarria, S., et al. (2021). Current Clinical Applications of In Vivo Gene Therapy with AAVs. *Mol. Ther.* 29, 464–488.
- Büning, H. (2013). Gene therapy enters the pharma market: the short story of a long journey. *EMBO Mol. Med.* 5, 1–3.
- Keeler, A.M., and Flotte, T.R. (2019). Recombinant Adeno-Associated Virus Gene Therapy in Light of Luxturna (and Zolgensma and Glybera): Where Are We, and How Did We Get Here? *Annu. Rev. Virol.* 6, 601–621.
- Heo, Y.A. (2023). Etranacogene Dezaparovec: First Approval. *Drugs* 83, 347–352.

7. Hamilton, B.A., and Wright, J.F. (2021). Challenges Posed by Immune Responses to AAV Vectors: Addressing Root Causes. *Front. Immunol.* *12*, 675897.
8. Ertl, H.C.J. (2022). Immunogenicity and toxicity of AAV gene therapy. *Front. Immunol.* *13*, 975803.
9. Muhuri, M., Levy, D.I., Schulz, M., McCarty, D., and Gao, G. (2022). Durability of transgene expression after rAAV gene therapy. *Mol. Ther.* *30*, 1364–1380.
10. Li, C., and Samulski, R.J. (2020). Engineering adeno-associated virus vectors for gene therapy. *Nat. Rev. Genet.* *21*, 255–272.
11. Gao, G.P., Alvira, M.R., Wang, L., Calcedo, R., Johnston, J., and Wilson, J.M. (2002). Novel adeno-associated viruses from rhesus monkeys as vectors for human gene therapy. *Proc. Natl. Acad. Sci. USA* *99*, 11854–11859.
12. Yao, Y., Wang, J., Liu, Y., Qu, Y., Wang, K., Zhang, Y., Chang, Y., Yang, Z., Wan, J., Liu, J., et al. (2022). Variants of the adeno-associated virus serotype 9 with enhanced penetration of the blood-brain barrier in rodents and primates. *Nat. Biomed. Eng.* *6*, 1257–1271.
13. Zhang, C., Yao, T., Zheng, Y., Li, Z., Zhang, Q., Zhang, L., and Zhou, D. (2016). Development of next generation adeno-associated viral vectors capable of selective tropism and efficient gene delivery. *Biomaterials* *80*, 134–145.
14. Yang, L., Jiang, J., Drouin, L.M., Agbandje-McKenna, M., Chen, C., Qiao, C., Pu, D., Hu, X., Wang, D.Z., Li, J., and Xiao, X. (2009). A myocardium tropic adeno-associated virus (AAV) evolved by DNA shuffling and in vivo selection. *Proc. Natl. Acad. Sci. USA* *106*, 3946–3951.
15. Deverman, B.E., Pravdo, P.L., Simpson, B.P., Kumar, S.R., Chan, K.Y., Banerjee, A., Wu, W.L., Yang, B., Huber, N., Pasca, S.P., and Gradinaru, V. (2016). Cre-dependent selection yields AAV variants for widespread gene transfer to the adult brain. *Nat. Biotechnol.* *34*, 204–209.
16. Nonnenmacher, M., Wang, W., Child, M.A., Ren, X.Q., Huang, C., Ren, A.Z., Tocci, J., Chen, Q., Bittner, K., Tyson, K., et al. (2021). Rapid evolution of blood-brain-barrier-penetrating AAV capsids by RNA-driven biopanning. *Mol. Ther. Methods Clin. Dev.* *20*, 366–378.
17. Tabebordbar, M., Lagerborg, K.A., Stanton, A., King, E.M., Ye, S., Tellez, L., Krunnusz, A., Tavakoli, S., Widrick, J.J., Messemmer, K.A., et al. (2021). Directed evolution of a family of AAV capsid variants enabling potent muscle-directed gene delivery across species. *Cell* *184*, 4919–4938.e22.
18. Ogden, P.J., Kelsic, E.D., Sinai, S., and Church, G.M. (2019). Comprehensive AAV capsid fitness landscape reveals a viral gene and enables machine-guided design. *Science* *366*, 1139–1143.
19. Zinn, E., Pacouret, S., Khaychuk, V., Turunen, H.T., Carvalho, L.S., Andres-Mateos, E., Shah, S., Shelke, R., Maurer, A.C., Plovie, E., et al. (2015). In Silico Reconstruction of the Viral Evolutionary Lineage Yields a Potent Gene Therapy Vector. *Cell Rep.* *12*, 1056–1068.
20. Gonzalez, T.J., Simon, K.E., Blondel, L.O., Fanous, M.M., Roger, A.L., Maysonet, M.S., Devlin, G.W., Smith, T.J., Oh, D.K., Havlik, L.P., et al. (2022). Cross-species evolution of a highly potent AAV variant for therapeutic gene transfer and genome editing. *Nat. Commun.* *13*, 5947.
21. Shay, T.F., Sullivan, E.E., Ding, X., Chen, X., Ravindra Kumar, S., Goertsen, D., Brown, D., Crosby, A., Vielmetter, J., Borsos, M., et al. (2023). Primate-conserved carbonic anhydrase IV and murine-restricted LY6C1 enable blood-brain barrier crossing by engineered viral vectors. *Sci. Adv.* *9*, eadg6618.
22. Kelemen, R.E., Mukherjee, R., Cao, X., Erickson, S.B., Zheng, Y., and Chatterjee, A. (2016). A Precise Chemical Strategy To Alter the Receptor Specificity of the Adeno-Associated Virus. *Angew. Chem., Int. Ed. Engl.* *55*, 10645–10649.
23. Yao, T., Zhou, X., Zhang, C., Yu, X., Tian, Z., Zhang, L., and Zhou, D. (2017). Site-Specific PEGylated Adeno-Associated Viruses with Increased Serum Stability and Reduced Immunogenicity. *Molecules* *22*, 1155.
24. Katrekar, D., Moreno, A.M., Chen, G., Worlikar, A., and Mali, P. (2018). Oligonucleotide conjugated multi-functional adeno-associated viruses. *Sci. Rep.* *8*, 3589.
25. Puzzo, F., Zhang, C., Powell Gray, B., Zhang, F., Sullenger, B.A., and Kay, M.A. (2023). Aptamer-programmable adeno-associated viral vectors as a novel platform for cell-specific gene transfer. *Mol. Ther. Nucleic Acids* *31*, 383–397.
26. Pipe, S.W., Leebeek, F.W.G., Recht, M., Key, N.S., Castaman, G., Miesbach, W., Lattimore, S., Peerlinck, K., Van der Valk, P., Coppens, M., et al. (2023). Gene Therapy with Etranacogene Dezaparvovec for Hemophilia B. *N. Engl. J. Med.* *388*, 706–718.
27. Liu, C.C., and Schultz, P.G. (2010). Adding new chemistries to the genetic code. *Annu. Rev. Biochem.* *79*, 413–444.
28. Chin, J.W. (2017). Expanding and reprogramming the genetic code. *Nature* *550*, 53–60.
29. Agbandje-McKenna, M., and Kleinschmidt, J. (2011). AAV capsid structure and cell interactions. *Methods Mol. Biol.* *807*, 47–92.
30. Ai, J., Ibrahim, R., Tai, P.W.L., and Gao, G. (2017). A Scalable and Accurate Method for Quantifying Vector Genomes of Recombinant Adeno-Associated Viruses in Crude Lysate. *Hum. Gene Ther. Methods* *28*, 139–147.
31. Santry, L.A., Ingrao, J.C., Yu, D.L., de Jong, J.G., van Lieshout, L.P., Wood, G.A., and Wootton, S.K. (2017). AAV vector distribution in the mouse respiratory tract following four different methods of administration. *BMC Biotechnol.* *17*, 43.
32. Grimm, D., Zhou, S., Nakai, H., Thomas, C.E., Storm, T.A., Fuess, S., Matsushita, T., Allen, J., Surosky, R., Lochrie, M., et al. (2003). Preclinical in vivo evaluation of pseudotyped adeno-associated virus vectors for liver gene therapy. *Blood* *102*, 2412–2419.
33. Liebler, J.M., Marconett, C.N., Juul, N., Wang, H., Liu, Y., Flodby, P., Laird-Offringa, I.A., Mino, P., and Zhou, B. (2016). Combinations of differentiation markers distinguish subpopulations of alveolar epithelial cells in adult lung. *Am. J. Physiol. Lung Cell Mol. Physiol.* *310*, L114–L120.
34. Halbert, C.L., Allen, J.M., and Miller, A.D. (2001). Adeno-associated virus type 6 (AAV6) vectors mediate efficient transduction of airway epithelial cells in mouse lungs compared to that of AAV2 vectors. *J. Virol.* *75*, 6615–6624.
35. Limberis, M.P., Vandenbergh, L.H., Zhang, L., Pickles, R.J., and Wilson, J.M. (2009). Transduction efficiencies of novel AAV vectors in mouse airway epithelium in vivo and human ciliated airway epithelium in vitro. *Mol. Ther.* *17*, 294–301.
36. van Lieshout, L.P., Domm, J.M., Rindler, T.N., Frost, K.L., Sorensen, D.L., Medina, S.J., Booth, S.A., Bridges, J.P., and Wootton, S.K. (2018). A Novel Triple-Mutant AAV6 Capsid Induces Rapid and Potent Transgene Expression in the Muscle and Respiratory Tract of Mice. *Mol. Ther. Methods Clin. Dev.* *9*, 323–329.
37. Seidel, L., Zarzycka, B., Zaidi, S.A., Katritch, V., and Coin, I. (2017). Structural insight into the activation of a class B G-protein-coupled receptor by peptide hormones in live human cells. *Elife* *6*, e27711.
38. Horowitz, E.D., Weinberg, M.S., and Asokan, A. (2011). Glycated AAV vectors: chemical redirection of viral tissue tropism. *Bioconjugate Chem.* *22*, 529–532.
39. Mével, M., Bouzelha, M., Leray, A., Pacouret, S., Guilbaud, M., Penaud-Budloo, M., Alvarez-Dorta, D., Dubreil, L., Gouin, S.G., Combal, J.P., et al. (2019). Chemical modification of the adeno-associated virus capsid to improve gene delivery. *Chem. Sci.* *11*, 1122–1131.
40. Liu, Y., Fang, Y., Zhou, Y., Zandi, E., Lee, C.L., Joo, K.I., and Wang, P. (2013). Site-specific modification of adeno-associated viruses via a genetically engineered aldehyde tag. *Small* *9*, 421–429.
41. Meyer-Berg, H., Zhou Yang, L., Pilar de Lucas, M., Zambrano, A., Hyde, S.C., and Gill, D.R. (2020). Identification of AAV serotypes for lung gene therapy in human embryonic stem cell-derived lung organoids. *Stem Cell Res. Ther.* *11*, 448.
42. Kang, M.H., van Lieshout, L.P., Xu, L., Domm, J.M., Vadivel, A., Renesme, L., Mühlfeld, C., Hurskainen, M., Miziková, I., Pei, Y., et al. (2020). A lung tropic AAV vector improves survival in a mouse model of surfactant B deficiency. *Nat. Commun.* *11*, 3929.
43. Westhaus, A., Cabanes-Creus, M., Rybicki, A., Baltazar, G., Navarro, R.G., Zhu, E., Drouyer, M., Knight, M., Albu, R.F., Ng, B.H., et al. (2020). High-Throughput In Vitro, Ex Vivo, and In Vivo Screen of Adeno-Associated Virus Vectors Based on Physical and Functional Transduction. *Hum. Gene Ther.* *31*, 575–589.
44. Goertsen, D., Goeden, N., Plytzanis, N.C., and Gradinaru, V. (2022). Targeting the lung epithelium after intravenous delivery by directed evolution of underexplored sites on the AAV capsid. *Mol. Ther. Methods Clin. Dev.* *26*, 331–342.
45. Weinmann, J., Weis, S., Sippel, J., Tulalamba, W., Remes, A., El Andari, J., Herrmann, A.K., Pham, Q.H., Borowski, C., Hille, S., et al. (2020). Identification of a myotropic AAV by massively parallel in vivo evaluation of barcoded capsid variants. *Nat. Commun.* *11*, 5432.

46. Hsu, H.L., Brown, A., Loveland, A.B., Lotun, A., Xu, M., Luo, L., Xu, G., Li, J., Ren, L., Su, Q., et al. (2020). Structural characterization of a novel human adeno-associated virus capsid with neurotropic properties. *Nat. Commun.* *11*, 3279.
47. Su, Q., Sena-Esteves, M., and Gao, G. (2020). Purification of Recombinant Adeno-Associated Viruses (rAAVs) by Cesium Chloride Gradient Sedimentation. *Cold Spring Harb. Protoc.* *2020*, 095604.
48. Berry, G.E., and Tse, L.V. (2017). Virus Binding and Internalization Assay for Adeno-associated Virus. *Bio. Protoc.* *7*, e2110.
49. Madigan, V.J., Yuziuk, J.A., Chiarella, A.M., Tyson, T.O., Meganck, R.M., Elmore, Z.C., Tse, L.V., Hathaway, N.A., and Asokan, A. (2019). Ring finger protein 121 is a potent regulator of adeno-associated viral genome transcription. *PLoS Pathog.* *15*, e1007988.